STABLE TEARING AND BUCKLING RESPONSES OF UNSTIFFENED ALUMINUM SHELLS WITH LONG CRACKS

James H. Starnes, Jr., and Cheryl A. Rose
NASA Langley Research Center
Hampton, VA 23681-0001, USA
Tel: (757) 864-3168
Fax: (757) 864-7791
j.h.starnes@larc.nasa.gov

ABSTRACT

The results of an analytical and experimental study of the nonlinear response of thin, unstiffened, aluminum cylindrical shells with a long longitudinal crack are presented. The shells are analyzed with a nonlinear shell analysis code that accurately accounts for global and local structural response phenomena. Results are presented for internal pressure and for axial compression loads. The effect of initial crack length on the initiation of stable crack growth and unstable crack growth in typical shells subjected to internal pressure loads is predicted using geometrically nonlinear elastic-plastic finite element analyses and the crack-tip-opening angle (CTOA) fracture criterion. The results of these analyses and of the experiments indicate that the pressure required to initiate stable crack growth and unstable crack growth in a shell subjected to internal pressure loads decreases as the initial crack length increases. The effects of crack length on the prebuckling, buckling and postbuckling responses of typical shells subjected to axial compression loads are also described. For this loading condition, the crack length was not allowed to increase as the load was increased. The results of the analyses and of the experiments indicate that the initial buckling load and collapse load for a shell subjected to axial compression loads decrease as the initial crack length increases. Initial buckling causes general instability or collapse of a shell for shorter initial crack lengths. Initial buckling is a stable local response mode for longer initial crack lengths. This stable local buckling response is followed by a stable postbuckling response, which is followed by general or overall instability of the shell.

1. INTRODUCTION

Transport fuselage shell structures are designed to support combinations of internal pressure and mechanical loads which can cause the structure to have a geometrically nonlinear structural response. These shell structures are required to have adequate structural integrity so that they do not fail if cracks develop during the service life of the aircraft. The structural response of a transport fuselage shell structure with a crack is influenced by the local stress and displacement gradients near the crack and by the internal load distribution in the shell. Local fuselage out-of-plane skin displacements near a crack can be large compared to the fuselage skin thickness, and these displacements can couple with the internal stress resultants in the shell to amplify the magnitudes of the local stresses and displacements near the crack. In addition, the stiffness and internal load distributions in a shell with a crack will change as the crack grows and when the skin buckles. This nonlinear response must be understood and accurately predicted in order to determine the structural integrity and residual strength of a fuselage structure with damage.

Fuselage shells are usually designed to allow the fuselage skin to buckle above a specified design load that can be less than the design limit load for the shell. During the design of the fuselage, it is assumed that the design limit load can occur anytime during the service life of the aircraft. As a result, a long crack could

exist in the fuselage shell after a considerable amount of flight service, and loading conditions could occur that cause the shell with the long crack to buckle. The results of a preliminary analytical study[1] of the effects of long cracks on the nonlinear response of unstiffened aluminum shells indicates that the behavior of a shell can be influenced significantly by the initial length of the crack.

The present paper describes the results of an analytical and experimental study of the effects of internal pressure and axial compression loads on the responses of thin, unstiffened, laboratory scale, aluminum cylindrical shells with a long longitudinal crack. Two wall thicknesses are considered in the analytical study to determine the effect of wall thickness on the shell response. The predicted effect of the initial crack length on the initiation of stable crack growth and on unstable crack growth is discussed for shells subjected to internal pressure loads. Stable crack growth is simulated using a geometrically nonlinear elastic-plastic finite element analysis and the crack-tip-opening angle (CTOA) fracture criterion. In addition, predicted prebuckling, buckling, and initial postbuckling results are presented and compared for cylindrical shells subjected to axial compression loads. The results presented illustrate the influence of the loading condition and initial crack length on shell crack-growth instabilities, and on shell buckling instabilities.

2. EXPERIMENTS

2.1 TEST SPECIMENS

The cylindrical shells tested in this investigation were fabricated from 0.040-inch-thick 2024-T3 bare aluminum alloy sheet, with the roll direction oriented circumferentially. All specimens were 39 inches long and 18 inches in diameter. Each specimen was fabricated with a 1.5-inch-wide double lap splice with 0.040-inch-thick splice plates and a single row of 0.1875-inch-diameter aluminum rivets on each side of the splice. The rivets were spaced 1.5 inches apart along the length of the specimens and were located five rivet diameters from the edges of the splice plates. A single longitudinal crack (0.010-inch-wide sawcut) was machined in each specimen at the specimen midlength, diametrically opposite to the lap splice. The initial cracks were either 2.0, 3.0 or 4.0 inches long. Specimens that were subjected to internal pressure loads had the crack tips sharpened with a razor blade to approximate a fatigue crack, and to insure some stable crack growth before the shells failed. To assure proper load introduction, and to assure that the ends of the cylinders remained circular during the tests, both ends of each specimen were potted in an aluminum-filled epoxy resin. The potting material extended 1.5 inches along the length from each end of the specimen, resulting in a test section length of 36 inches. The ends of the specimens subjected to compression loads were machined flat and parallel.

2.2 APPARATUS, INSTRUMENTATION AND TEST PROCEDURE

The specimens subjected to axial compression were loaded with a controlled end-shortening displacement using a 300-kip hydraulic test machine. Before each test a load balancing procedure was employed to assure that the load was applied to the specimens as uniformly as possible. All compression specimens were loaded to the point of global collapse. Specimens subjected to internal pressure loads were attached to end fittings, and slowly pressurized to failure with nitrogen gas. Details of the shell specimen and the end fittings are shown in Fig. 1. Two end plates with O-ring seals maintained internal pressure in the shell. A pressure line was attached to one end of the specimen and an instrumentation terminal block was attached to the other. One end ring of the specimens was clamped to rigid beams on the ground, and the other end was unconstrained in the axial direction to allow free expansion of the specimen.

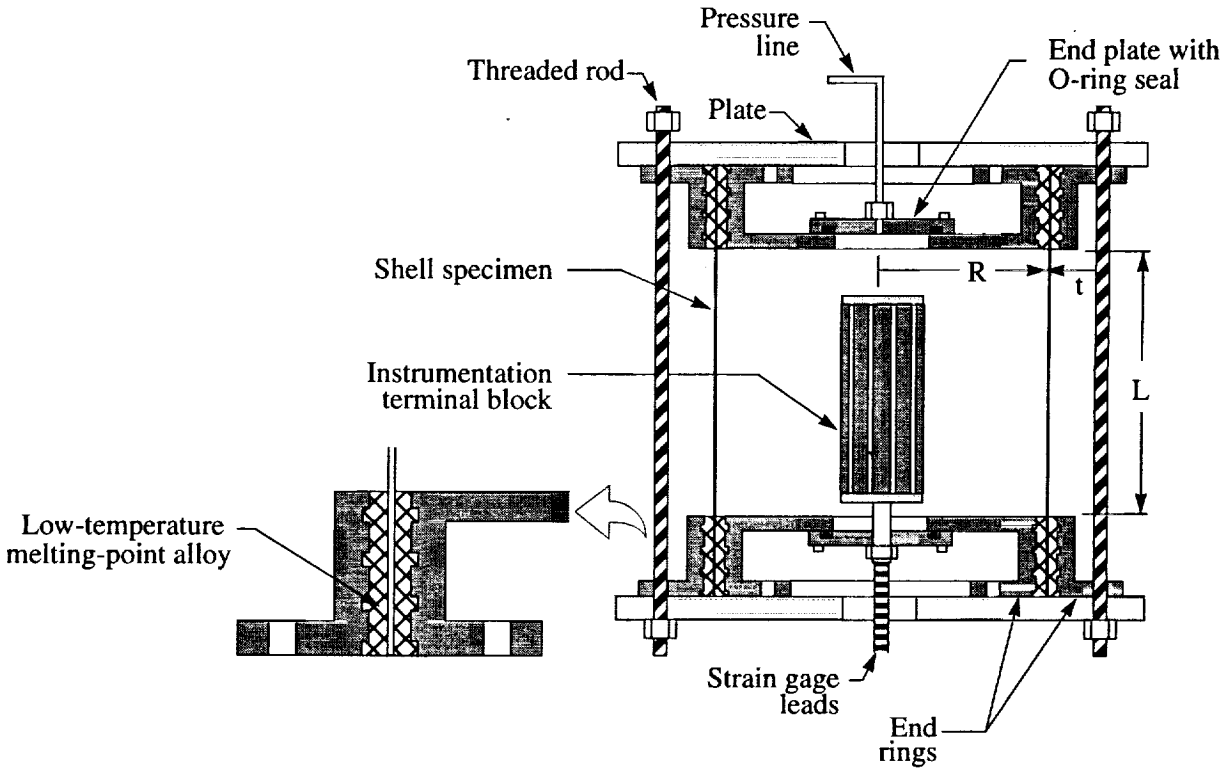

Figure 1. Schematic of pressure test shell specimen.

All specimens were instrumented with back-to-back electrical resistance strain gages mounted on the internal and external surfaces of the cylinder. Crack wire gages were applied at a crack tip of the specimens subjected to internal pressure loads to record the stable crack growth response of the crack. A moiré interferometry procedure was used with the compression-loaded specimens to observe the deformation patterns before and after buckling had occurred. Three non-collinear direct current differential transducers were used to measure the displacements of the loading platen for the compression loaded specimens. All data were recorded with a data acquisition system, and the response of all specimens was recorded on video tape.

3. SHELL MODELS AND ANALYSIS PROCEDURES

3.1 SHELL MODELS

The geometry of the shells analyzed in this study is defined in Fig. 2a. The shells have a 9.0-inch radius, R, a 0.040- or 0.020-inch-thick wall, t, and a 36.0-inch unsupported length, L. A longitudinal crack is located at $\theta = 0°$ and at shell mid length. The initial crack length, a, ranges from 1.0 to 4.0 inches. The shells are typical laboratory-scale cylindrical shells and are made of 2024-T3 bare aluminum alloy, with the sheet rolling direction oriented in the circumferential direction.

The finite element models used to simulate the response of the cracked shells subjected to internal pressure and axial compression loads are shown in Fig. 2b and Fig. 2c, respectively. For the internal pressure load case, advantage was taken of the symmetry of the problem, and only a quarter of the shell was modeled.

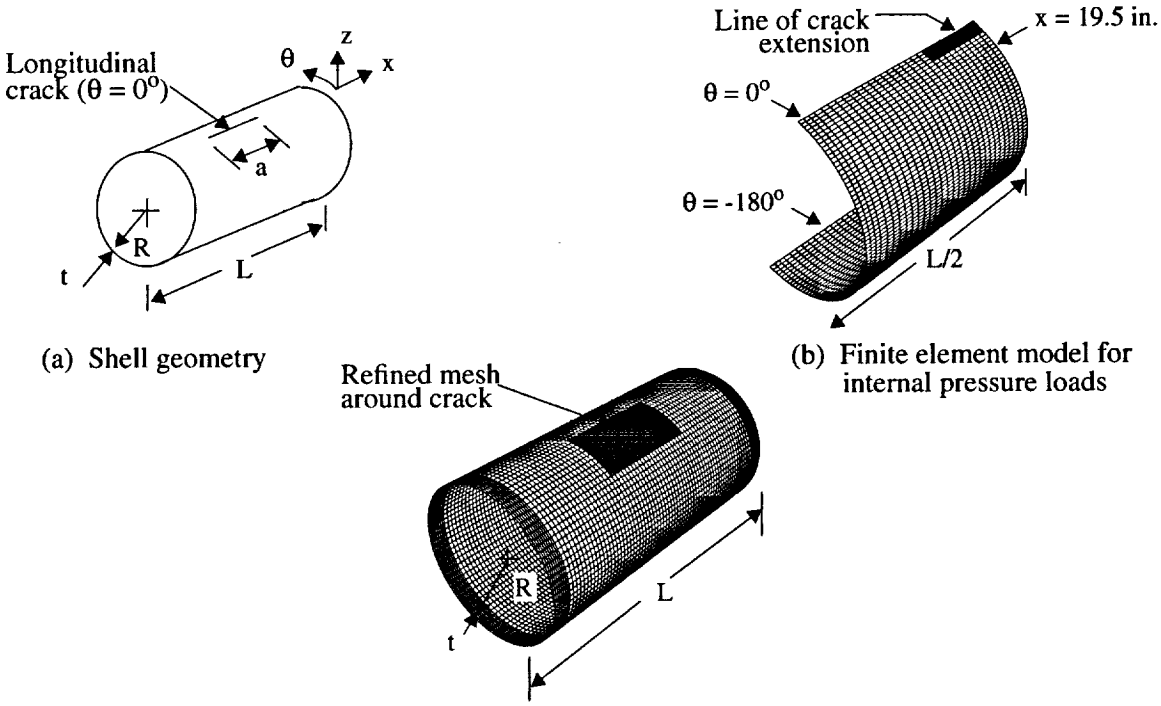

Figure 2. Shell geometry and finite element models.

Symmetry conditions were applied along the edges $\theta = 0°$ and $\theta = -180°$ and along the edge $x = 19.5$ inches. Self-similar crack growth was assumed; therefore, straight cracks with initial half-lengths of 0.5 to 2.0 inches were defined in the model along $\theta = 0°$ and extended from the symmetry boundary at the edge, $x = 19.5$ inches. Mesh refinement was used to provide elements with side lengths equal to 0.04 inches along the line of crack extension. This mesh density was required to predict accurately the crack extension using the CTOA criterion.[2] The shells were modeled using STAGS standard quadrilateral shell elements and mesh-transition elements, to transition from the very refined mesh around the crack to a course mesh remote from the crack. Each of the shell element nodes has six degrees of freedom, including three translational degrees of freedom, u, v, and w, and three rotational degrees of freedom, about the axes x, θ, and z. Internal pressure was simulated by applying a uniform lateral pressure to the shell wall and an axial tensile force to the end of the shell at $x = 0.0$ inches. Multi-point constraints were used to enforce a uniform end displacement. The circumferential and radial degrees of freedom, v and w, respectively, were constrained in regions of the cylinder 0.0 in. $\leq x \leq$ 1.5 in. to approximate the experimental end conditions.

The entire cylindrical shell was modeled for the axial compression load case. The finite element model for this load case is shown in Fig. 2c. Straight cracks with initial lengths of 1.0 to 4.0 inches were defined in the model along $\theta = 0°$ and at the shell midlength. The primary objective of the study for the axial compression load case was to continue the analysis beyond the critical buckling state, and to focus on the post-buckling response of the shell with a crack. Thus, the interaction between local buckling and crack extension was not specifically addressed; that is, the crack lengths were held constant throughout the analyses. Therefore, the mesh was not as refined in the vicinity of the crack for this load case as it was for the internal pressure load case. The compression load was applied to the ends of the shell by specifying a uniform end displacement. As in the pressure load case, the circumferential and radial degrees of freedom, v and w, respectively, were constrained in regions of the cylinder 0.0 in. $\leq x \leq$ 1.5 in. to approximate the experimental end conditions.

3.2 NONLINEAR ANALYSIS PROCEDURE

The shell responses were predicted numerically using the STAGS (STructural Analysis of General Shells) nonlinear shell analysis code.[3] STAGS is a finite element code for general-purpose analysis of shells of arbitrary shape and complexity. STAGS analysis capabilities include stress, stability, vibration and transient response analyses, with both material and geometric nonlinearities represented. The code uses both the modified and full Newton methods for its nonlinear solution algorithms, and accounts for large rotations in a shell by using a co-rotational algorithm at the element level. The Riks pseudo arc-length path following method[4,5] is used to continue a solution past the limit points of a nonlinear response.

STAGS can also perform crack-propagation analyses, and can represent the effects of crack growth on nonlinear shell response. A nodal release method and a load-relaxation technique are used to extend a crack while the shell is in a nonlinear equilibrium state.[6] The condition for crack extension is based upon a fracture criterion. When a crack is to be extended, the forces necessary to hold the current crack tip nodes together are calculated. The crack is extended by releasing the nodal compatibility condition at the crack tip, applying the equivalent crack-tip forces, and then releasing these forces to establish a new equilibrium state, which corresponds to the longer crack. The changes in the stiffness matrix and the internal load distribution that occur during crack growth are accounted for in the analysis, and the nonlinear coupling between internal forces and in-plane and out-of-plane displacement gradients that occurs in a shell is properly represented. Output from STAGS, associated with a crack, includes the strain-energy-release rate in an elastic analysis, and the crack-tip-opening angle (CTOA) in an elastic-plastic analysis. These quantities can then be used as part of a fracture criterion in an elastic analysis or an elastic-plastic analysis to predict stable crack growth and the residual strength of a damaged shell.

3.2.1 Internal Pressure Load

An elastic-plastic STAGS analysis, using the nodal release method and load relaxation technique described above to extend the crack, was used to predict the residual strength of the cracked pressurized cylinders. The material nonlinearity was represented by the White-Besseling mechanical sublayer distortional energy plasticity theory used in STAGS. A piecewise linear representation was used for the uniaxial stress strain curve for 2024-T3 aluminum (Fig. 3).[7]

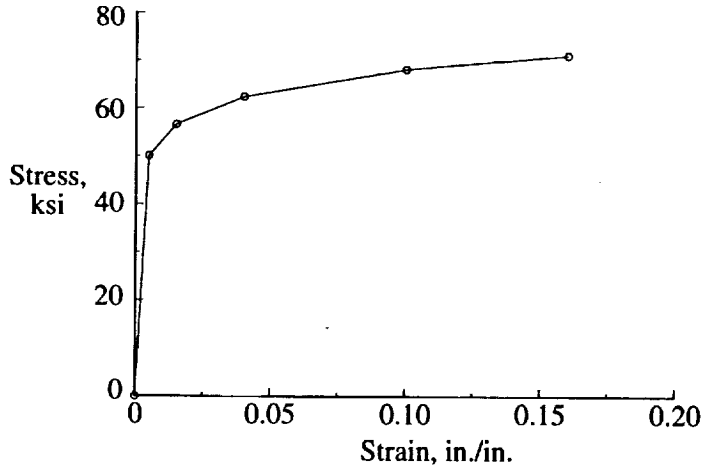

Stress (ksi)	Strain (in./in.)
0.00	0.00
50.0	0.0048
56.6	0.015
62.3	0.040
68.2	0.100
71.1	0.160

E = 10.35 Msi
ν = 0.3

Figure 3. Piecewise linear representation for the uniaxial stress-strain curve for 2024-T3 aluminum (L-T orientation).

The critical crack-tip-opening angle (CTOA) fracture criterion[2,7,8] was used to simulate stable crack growth. The CTOA fracture criterion uses the crack opening angle, shown schematically in Fig. 4, as the fracture parameter. The CTOA, evaluated at a fixed distance from the moving crack tip, is defined as the angle made by the upper crack surface, the crack tip, and the lower crack surface. In the present study, the CTOA was evaluated at a distance of 0.04 inches behind the crack tip. Newman[2] has shown this value to be adequate for analyzing stable crack growth in a wide variety of materials. The criterion assumes that crack growth will occur when the angle reaches a critical value, $CTOA_{cr}$, and that the critical value will remain constant as the crack extends. These assumptions are supported by experimental studies and numerical elastic-plastic finite element analyses that have shown that, in several metals, the CTOA is essentially constant after some initial crack growth.[7] The value of the critical angle is dependent on the sheet material, the sheet thickness and the crack orientation, and can be determined from three-dimensional, elastic-plastic, finite element simulations of the fracture behavior of small laboratory specimens. The determined angle can then be used to predict the fracture behavior of different structural configurations. In a two-dimensional, plane stress, elastic-plastic finite element analysis, the accuracy of residual strength predictions obtained using the $CTOA_{cr}$ determined as described above, is affected by the panel width. This dependence on panel width is postulated to be caused by three-dimensional constraint effects that develop near the crack tips.[9] To eliminate the dependence of the two-dimensional plane stress finite element analysis on the structural configuration, the three-dimensional constraint effects are approximated in the two-dimensional model by incorporating a "core" of plane strain elements on each side of the crack line (see Fig. 4). The dimension of the plane strain core region on each side of the crack line is referred to as the plane strain core height, h_c. The value of h_c can be determined by correlating two-dimensional, elastic-plastic finite element analysis results, that use the $CTOA_{cr}$ determined from three-dimensional finite element analysis, with experimental results for small laboratory specimens. The procedure used in the present study for determining the values of $CTOA_{cr}$ and h_c is described in more detail in Section 3.3.

The prebuckling, buckling and postbuckling responses of the shells for the axial compression loading condition were determined using the following analysis procedure. The prebuckling responses were determined using the geometrically nonlinear quasi-static analysis capability in STAGS. The initial, unstable, postbuckling response of the shell was predicted using the nonlinear transient analysis option of the code. The transient analysis was initiated from an unstable equilibrium state just beyond the buckling point by increasing the end-shortening displacement. The transient analysis was continued until the transient response damped out or decayed. Once the transient analysis converged to a steady-state solution, the load relaxation option of the code was used to establish a stable equilibrium state. The subsequent stable postbuckling response of the shell was computed using the standard nonlinear, static analysis option. For the parametric studies presented in Section 4.2, plasticity effects were not included in the analyses. However, elastic-plastic analyses were conducted to provide a preliminary assessment of the effects of plasticity on the shell buckling response, and for comparison with the experimental results.

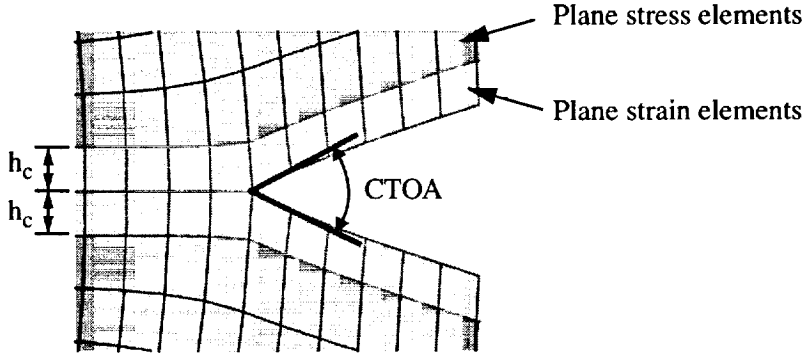

Figure 4. Schematic for fracture parameters, $CTOA_{cr}$ and h_c.

3.3 DETERMINATION OF $CTOA_{cr}$ AND h_c

Fracture tests of compact tension, C(T), and middle crack tension, M(T), specimens were conducted by the Mechanics of Materials Branch at NASA Langley Research Center. The test specimens were made of the same 0.040-inch-thick 2024-T3 aluminum sheet material that was used for the cylinders. The specimens were fatigue cracked, or notched, with the crack perpendicular to the sheet rolling direction. The C(T) specimens were 6 inches wide, with an initial crack length, a, equal to 2.4 inches. The M(T) specimens were 12 inches wide, with an initial crack length, a, equal to 4 inches. For the notched specimens, the tips were sharpened with a razor blade to produce crack tips similar to the crack tips in the pressurized cylinder test specimens. A residual strength test of each specimen was conducted under displacement control loading conditions. Guide plates, to constrain out-of-plane deformations, were used during the residual strength tests of all of the C(T) specimens and of one of the fatigue cracked M(T) specimens. Load, crack extension, and surface crack opening displacement measurements were made during the tests. The fracture behavior of the unconstrained M(T) panel with the razor blade sharpened notch was basically identical to the behavior of the unconstrained M(T) panels with fatigue cracks.

The fracture parameters that were used in the residual strength analysis of the pressurized cylinders were determined by simulating the fracture behavior of the C(T) and M(T) tests. Personnel from the Mechanics of Materials Branch conducted three-dimensional, geometrically linear, finite element simulations, with the ZIP3D code,[10,11] to determine the $CTOA_{cr}$ that best correlated the experimental results for the constrained C(T) and M(T) tests. In the three-dimensional analyses, the three dimensional constraint effects at the crack tip are directly modeled, and the core height parameter, h_c, is eliminated. The angle determined from the three-dimensional analyses was then used in a geometrically linear, two-dimensional simulation performed using the ZIP2D code[12,13] to determine the core height, h_c, that best correlated the experimental results for the constrained M(T) and C(T) tests. The fracture parameters determined in this manner for 0.040-inch-thick 2024-T3 bare aluminum, for fracture in the L-T orientation, had a $CTOA_{cr}$ equal to 5.6 degrees and a plane strain core height equal to 0.04 inches.

To verify application of these parameters in a STAGS analysis, elastic-plastic, geometrically nonlinear STAGS analyses were conducted for the C(T) tests, and for the constrained and unconstrained M(T) tests. The mesh used in the analysis was refined to provide elements along the line of crack extension with side lengths equal to 0.04 inches. Predicted and measured load results for the C(T) and M(T) panels are shown in Fig. 5 for increasing values of crack extension, Δa. These results indicate that the STAGS analysis accurately predicted the stable tearing and residual strength for the C(T) and for the M(T) panels with buckling constrained. The STAGS analysis for the unconstrained M(T) specimens predicted accurately the early portion of the crack extension. However, some discrepancy was observed in the analysis predictions and experimental results for the latter portion of crack extension, and the residual strength of these tests was overpredicted by approximately 9%. This discrepancy is consistent with the differences that have been observed in test and analysis results of wider and thicker, unstiffened sheets. Additional studies are required to resolve this issue.

4. RESULTS AND DISCUSSION

The nonlinear analysis and test results for thin unstiffened aluminum cylindrical shells with a longitudinal crack are presented in this section. Results have been generated for two loading conditions: internal pressure only, and axial compression only. Results for these loading conditions are presented for shells with a longitudinal crack at shell midlength and with initial crack lengths of 1.0, 2.0, 3.0 and 4.0 inches. The maximum value of the applied internal pressure considered is 143 psi. This pressure is the pressure required to cause a shell with a 1.0-inch-long initial crack and a 0.040-inch wall thickness to fail due to an internal pressure load. The axial compression loads are increased from zero to the maximum axial load that the shell can

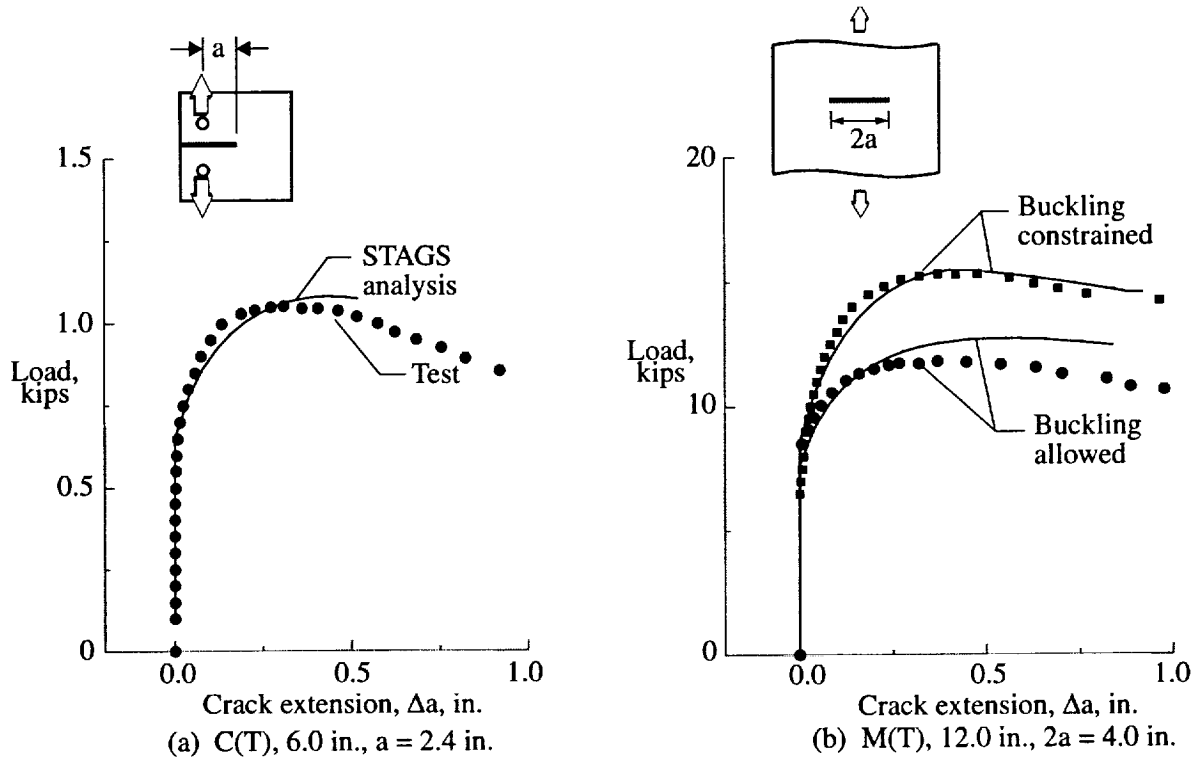

Figure 5. STAGS analysis predictions and test results for C(T) and M(T) panels.

support. Typical results are presented to illustrate the effects of crack length on the crack growth response of a shell subjected to internal pressure loads, and on the prebuckling, buckling and postbuckling responses of a shell subjected to axial compression loads. Shells with both 0.020- and 0.040-inch wall thicknesses are considered for the analysis results, but only shells with a 0.040-inch wall thickness are considered for the experimental results.

4.1 INTERNAL PRESSURE LOADS

The effect of increasing the internal pressure in a shell on the total crack growth or crack extension is shown in Fig. 6a and Fig. 6b for shells with initial crack lengths of 1.0, 2.0, 3.0, and 4.0 inches, and with wall thicknesses of 0.040 and 0.020 inches, respectively. These results were generated using the mesh shown in Fig. 2b, and a STAGS plane stress analysis, prior to determining the fracture parameters $CTOA_{cr}$ and h_c from the C(T) and M(T) tests. Therefore, a preliminary critical crack-tip-opening angle was determined by correlating the results of a STAGS plane stress analysis of a cylinder with an initial 4.0-inch-long longitudinal crack with the experimentally observed behavior of an aluminum shell of the same geometry. The critical crack-tip-opening angle determined in this manner, and used in all of the parametric studies, was 5.36°. The results in Fig. 6 indicate that the internal pressure in the shell can be increased, and the cracked shell will remain in equilibrium, up to a pressure at which yielding occurs at the crack tips and the opening angle at the crack tips reaches a critical value. At this pressure, the crack will start to grow. The initial growth of the crack is stable and the crack will not extend unless the pressure is increased. Eventually, unstable crack growth occurs. Unstable growth occurs when the slope of the curves in Figs. 6a and 6b becomes zero, which means that a small increase in pressure causes a very large increment in crack extension.

The effect of increasing the initial crack length on the internal pressure required to initiate stable crack growth and on the pressure at which stable growth changes to unstable crack growth is summarized in Fig. 6c for the two shell wall thicknesses. The solid curve for each shell wall thickness represents the pressure

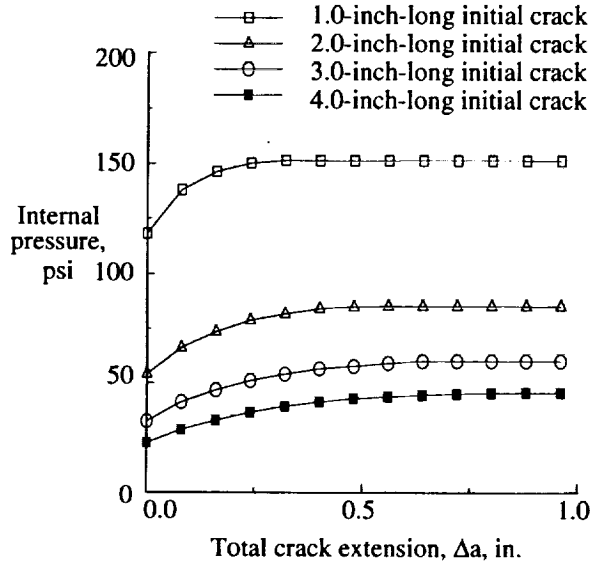

(a) Crack extension for 0.040-inch-thick shells

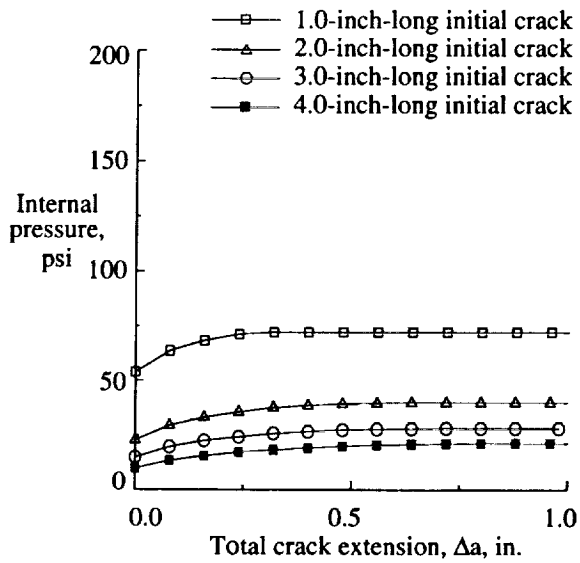

(b) Crack extension for 0.020-inch-thick shells

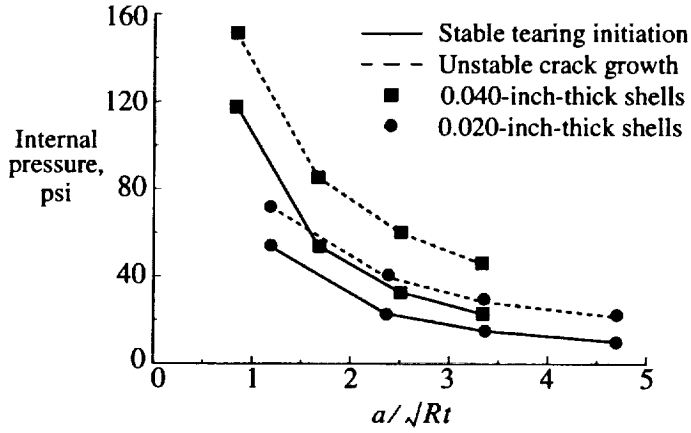

(c) Initial stable tearing and unstable crack growth

Figure 6. Effect of increasing internal pressure on initial stable crack growth and unstable crack growth for different initial crack lengths.

required to initiate stable crack growth as a function of normalized initial crack length, and the dashed curve for each shell wall thickness represents the pressure that causes the crack growth to become unstable. These results indicate that the internal pressure required to initiate stable crack growth and to cause unstable crack growth decreases as the initial crack length increases. The results shown in Fig. 6c also indicate that the difference between the internal pressure required to initiate stable crack growth and the internal pressure that causes unstable crack growth decreases as the initial crack length increases. For an initial crack length of 1.0 inch, stable crack growth initiates in the 0.040-inch-thick shell when the internal pressure is approximately 113 psi, and unstable crack growth occurs when the internal pressure is approximately 143 psi. The difference between the internal pressure required to initiate stable crack growth and the internal pressure that causes unstable crack growth is approximately 30 psi for the 1.0-inch initial crack length in the 0.040-inch-thick shell. The results for an initial crack length of 2.0 inches in the 0.040-inch-thick shell indicate that stable crack growth initiates when the internal pressure is approximately 51 psi, and unstable crack growth occurs when the internal pressure is approximately 79 psi. The difference between the internal pressure required to initiate stable crack growth and the internal pressure that causes unstable crack growth for

this initial crack length is 28 psi. The difference between the internal pressure required to initiate stable crack growth and the internal pressure that causes unstable crack growth for the 3.0- and 4.0-inch initial crack lengths in the 0.040-inch-thick shell is approximately 24 psi and 21 psi, respectively. The results for the 0.020-inch-thick shell are similar, but with lower values of internal pressure.

The results from the nonlinear analyses indicate that the internal pressure load induces large outward radial displacements in the neighborhood of the crack. The response associated with these radial displacements is often referred to as "crack bulging" in the literature and is the cause of the larger crack opening displacements and crack-tip stress-intensity factors in a shell, compared to those for a flat sheet under otherwise identical conditions.[14] Furthermore, the extent of crack bulging is a function of the nondimensional crack curvature parameter, $a/\sqrt{Rt}$. This observation is illustrated for the 0.040-inch-thick shell in Fig. 7, which shows the radial displacement response along the shell length at the circumferential location $\theta = 0°$, just before the initiation of stable crack growth, for each of the initial crack lengths. The radial displacement at the center of the crack normalized by the shell thickness, t, is w_o/t =1.00, 1.65, 2.38 and 3.23 for the 1.0-, 2.0-, 3.0- and 4.0-inch-long initial cracks, respectively. These displacements are greater than or equal to the shell wall thickness for all of the crack lengths considered, and represent large displacements in the context of nonlinear thin shell theory. The increase in crack bulging for the longer initial crack lengths is consistent with the observation that the pressure required to initiate stable crack growth decreases with the increase in initial crack length.

Experimental and analytical results for the 0.040-inch-thick shells are compared in Fig. 8 and Fig. 9. The analytical results were generated using the fracture parameters determined as described in Section 3.3. The experimental and predicted strains in the skin at three locations near the crack tip are compared in Fig. 8. The correlation between the predicted and experimentally determined strains indicates that the finite element model accurately simulates the stress state near the crack tip. The effect of internal pressure on the analytical and experimental crack growth results is shown in Fig. 9 for shells with initial crack lengths equal to 2.0, 3.0, and 4.0 inches. The analytical and experimental residual strength results correlate very well for all crack lengths. However, in all cases, the analysis overpredicts the initial portion of the crack growth response.

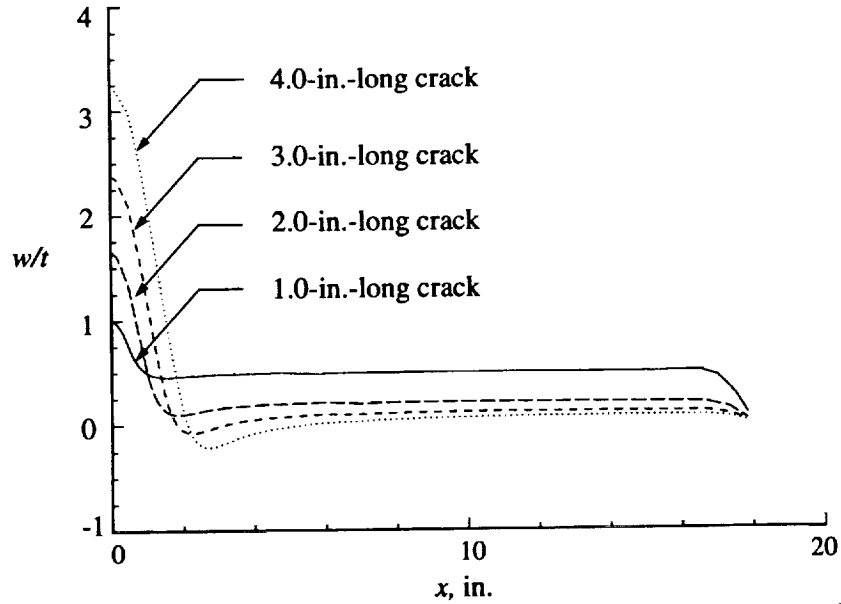

Figure 7. Radial displacement response along the shell length at the circumferential location θ = 0°, just before the initiation of stable crack growth for 0.040-inch-thick shells.

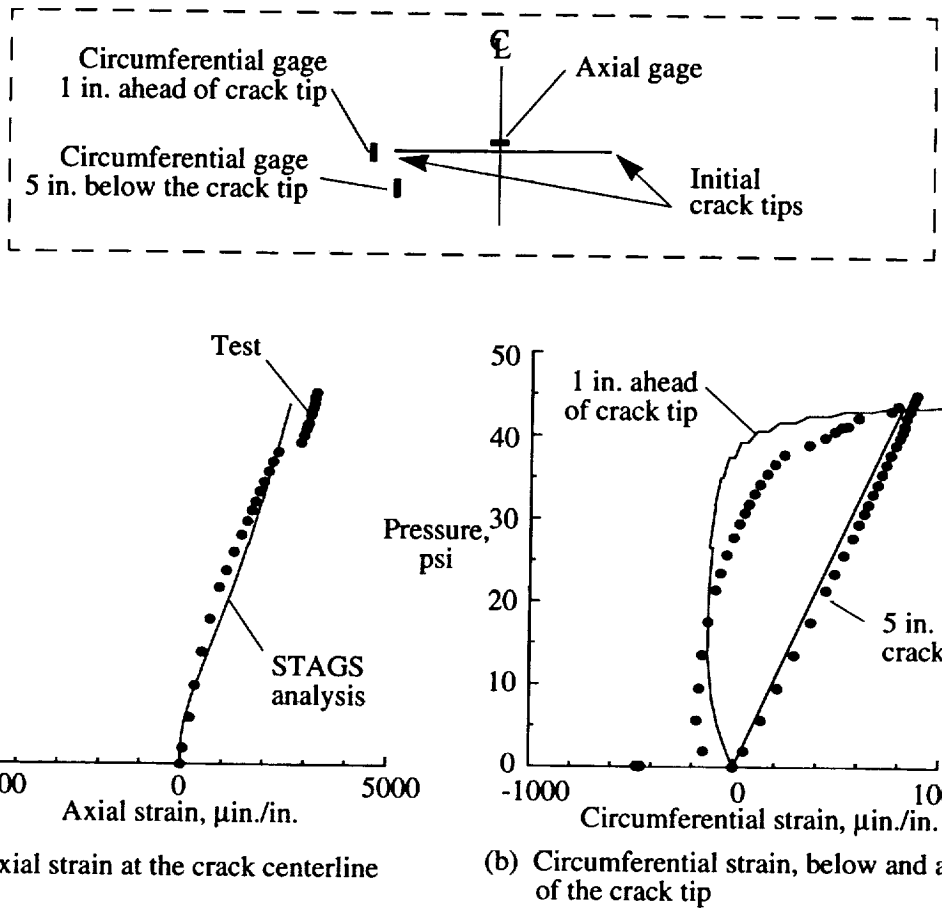

(a) Axial strain at the crack centerline

(b) Circumferential strain, below and ahead of the crack tip

Figure 8. Comparison of experimental and predicted strain response for a shell with a 4.0-inch-long initial crack.

4.2 AXIAL COMPRESSION LOADS

The predicted load-shortening responses for a 0.040-inch-thick shell and a 0.020-inch-thick shell with initial crack lengths of 1.0, 2.0, 3.0 and 4.0 inches and subjected to axial compression are shown in Figs. 10a and 10b, respectively. An initial outward geometric imperfection in the form of the lowest eigenmode was used in the nonlinear analyses to generate local deformations in the vicinity of the crack. The applied compression and end-shortening values are normalized by the corresponding classical buckling values for a shell without a crack. For the 0.040-inch-thick shell and the 0.020-inch-thick shell with a 1.0-inch-long crack, the crack introduces an effective imperfection that causes general instability to occur at the loads indicated by the **X** in Figs. 10a and 10b. These shells cannot support additional compression load after buckling. For a shell with a longer crack, local buckling near the crack precedes shell collapse. The filled symbols in Figs. 10a and 10b identify the loads that correspond to initial local buckling near the crack for the 0.040-inch-thick shell and the 0.020-inch-thick shell, respectively, with the 2.0-, 3.0-, and 4.0-inch-long initial cracks. Prior to buckling the radial displacement, w_o, at the center of the crack edges is nearly equal to zero. Once the critical load is reached, w_o increases rapidly as the load increases. Initial local buckling is followed by a stable postbuckling response, and the load can be further increased after local buckling has occurred near the crack edges.

As the load is increased after initial local buckling has occurred, the 0.040-inch-thick shells with the 3.0- and 4.0-inch-long cracks, and the 0.020-inch-thick shells with the 2.0-, 3.0-, and 4.0-inch-long cracks ex-

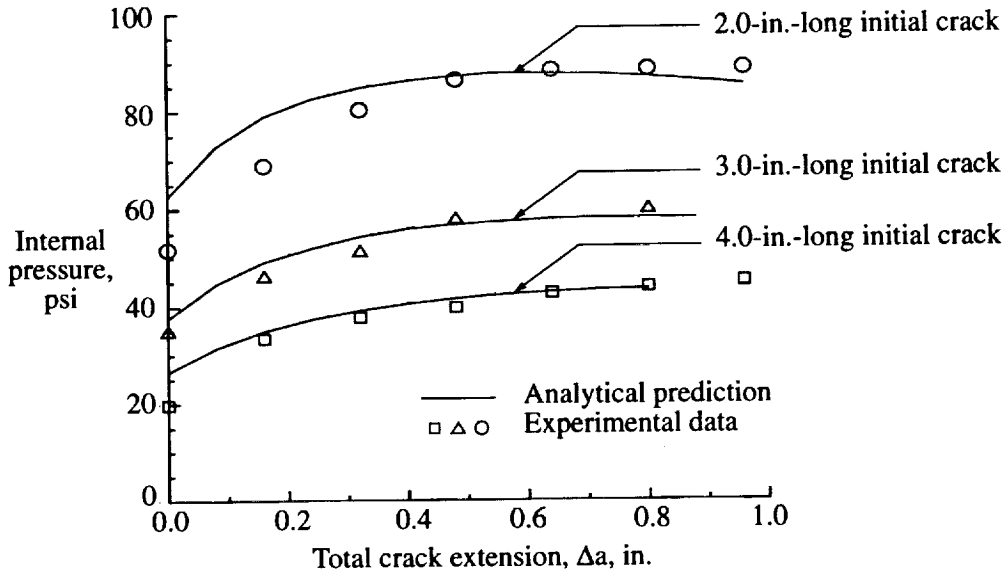

Figure 9. Comparison of analytical and experimental total crack extension results for 0.040-inch-thick internally pressurized shells.

perience a change in the local buckling mode. The initial postbuckling response of the shells after the mode change is unstable, and as a result, the axial load decreases after buckling occurs. The unstable transition region in the response predictions is indicated by the broken lines in Figs. 10a and 10b. The unstable transition from the stable initial buckled configuration to the stable postbuckling configuration was determined by using the transient analysis capability in STAGS. The transient analysis was continued until the kinetic energy in the system was small. A time history of the kinetic energy during the transient analysis of the 0.040-inch-thick shell with a 3.0-inch-long crack is shown in Fig. 11. The deformed shapes labeled A, B, C and D in Fig. 11 correspond to the points A, B, C and D on the load-end shortening and kinetic energy history curves, and show the development of the shell's postbuckled response. Point A corresponds to the initial buckling deformation, points B and C correspond to solutions obtained during the transient analysis, and point D represents the stable postbuckled equilibrium state. Once a stable equilibrium state was determined from the transient analysis, the nonlinear static analysis was resumed to compute the stable postbuckling equilibrium response results shown in Fig. 10a. The analysis was continued for the shells with the 3.0- and 4.0-inch-long cracks for the 0.040-inch-thick shells, and for the shells with the 2.0-, 3.0-, and 4.0-inch-long cracks for the 0.020-inch-thick shells until computational convergence problems were encountered. The load corresponding to the onset of these convergence difficulties is assumed to correspond to shell collapse. Collapse of the 0.040-inch-thick and of the 0.020-inch-thick shells with 2.0-, 3.0- and 4.0-inch-long cracks is identified by the open symbols in Figs. 10a and 10b, respectively.

The initial local buckling load predictions and qualitative approximations for the shell collapse load for the 0.020- and 0.040-inch-thick shells are summarized in Fig. 10c. The predicted collapse loads for the shells are only qualitative approximations because they were assumed to correspond to the point of onset of convergence difficulties in the elastic analyses, and, as will be shown subsequently, the collapse loads for the shells with the longer cracks may be affected by material nonlinear response. The values of the normalized initial buckling loads for the 0.040-inch-thick shells are P/P_{cr} = 0.88, 0.54, 0.39, and 0.32, and the qualitative approximate values of the normalized collapse loads are P/P_{cr} = 0.88, 0.59, 0.49, and 0.47 for the 1.0-, 2.0-, 3.0- and 4.0-inch-long cracks, respectively. The values of the normalized initial buckling loads for the 0.020-inch-thick shells are P/P_{cr} = 0.73, 0.41, 0.30, and 0.24, and the qualitative approximate values of the normalized collapse loads are P/P_{cr} = 0.73, 0.47, 0.43, and 0.41 for the 1.0-, 2.0-, 3.0- and 4.0-

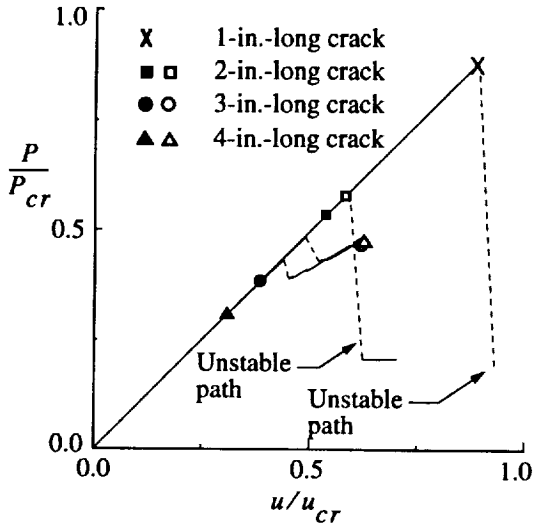

(a) Load-shortening response for 0.040-inch-thick shells

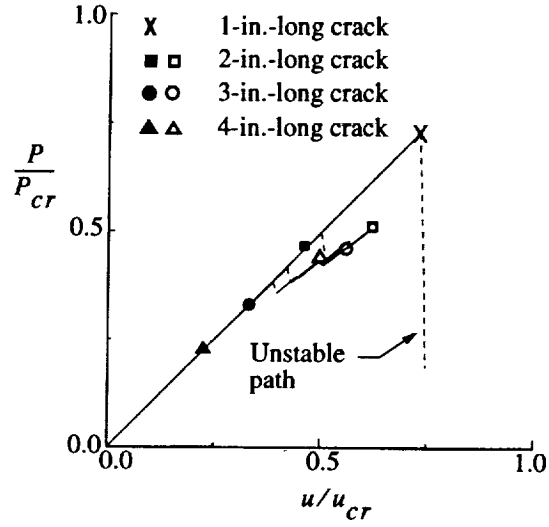

(b) Load-shortening response for 0.020-inch-thick shells

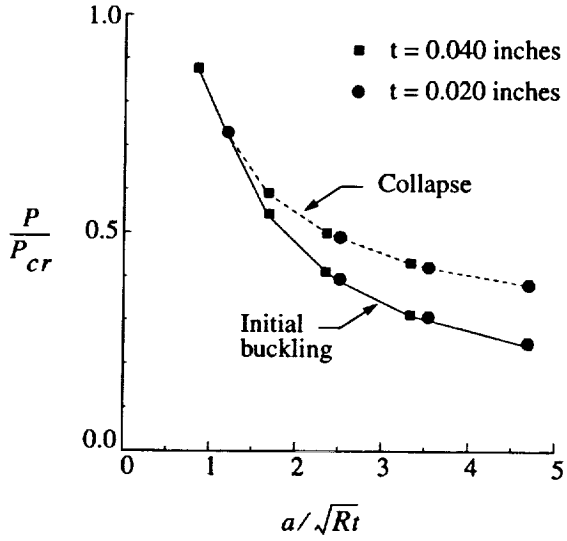

(c) Initial buckling and collapse loads

Figure 10. Effect of initial crack length on the response of cylindrical shells with longitudinal cracks and subjected to axial compression.

inch-long cracks, respectively. These results indicate that the magnitudes of the initial buckling loads and collapse loads for the shells decrease as the initial crack length increases. In addition, the difference between the load at initial buckling and the load at collapse is smaller for the shorter crack lengths. The initial local buckling load results for the 0.020- and 0.040-inch-thick shells are represented very well by a characteristic curve that is based on the curvature parameter $a/\sqrt{Rt}$.

The effects of material nonlinearities on the predicted load-shortening response and deformation patterns for a 0.040-inch-thick shell with a 3.0-inch-long crack are shown in Fig. 12. Initial plastic yielding occurs for an applied load corresponding to $P/P_{cr} = 0.43$, which is approximately 90 percent of the buckling load corresponding to the local mode change. The load-shortening predictions based upon an elastic analysis and an elastic-plastic analysis, and the deformation pattern prediction just prior to the local mode change, indicate that the shell response prior to the local mode change is adequately predicted by an elastic analysis

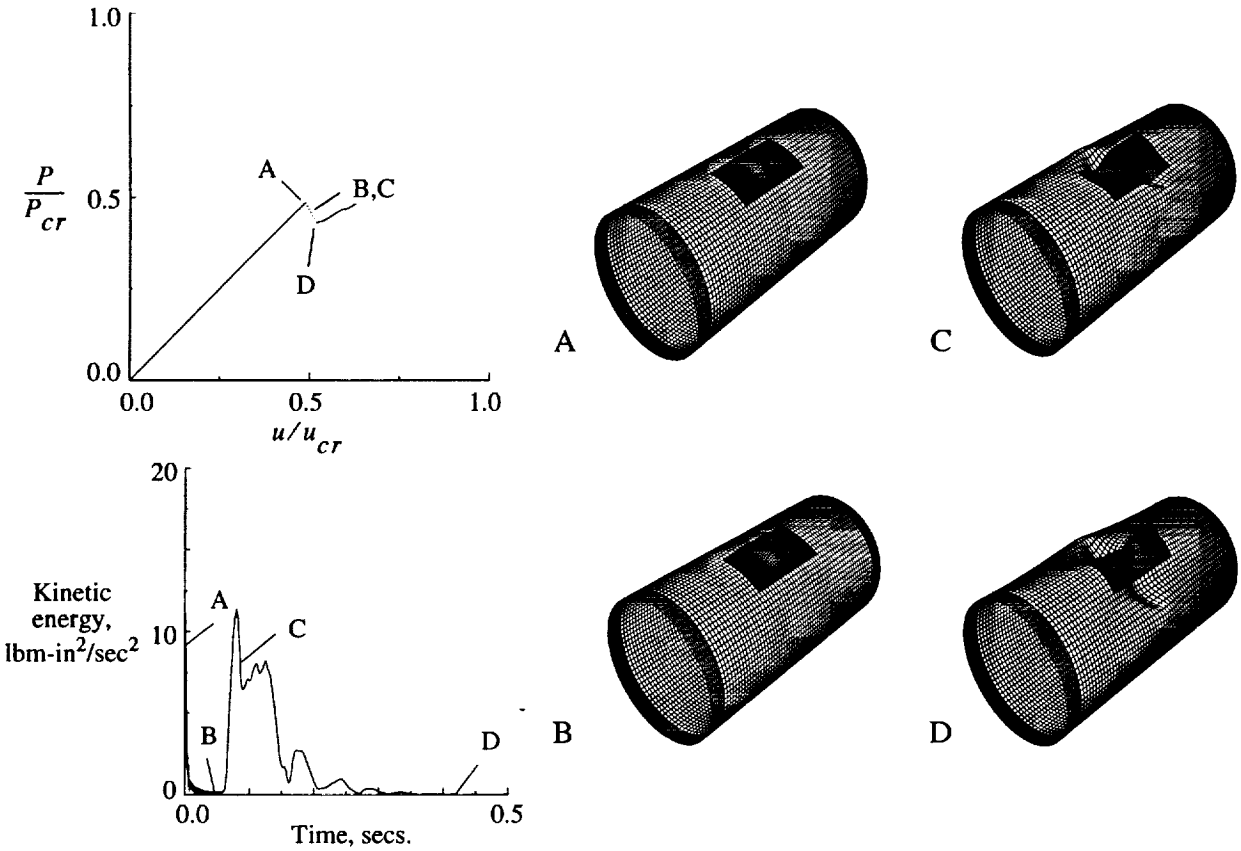

Figure 11. Transient analysis results for the unstable buckling response of a 0.040-inch-thick shell with a 3.0-inch-long crack and subjected to axial compression.

(Figs. 12a and 12b). The initial postbuckled response predictions of the two analyses are, however, significantly different. The initial postbuckled deformation pattern prediction from the elastic-plastic analysis, corresponding to Point B in Fig. 12a, is shown in Fig. 12c, and the initial postbuckled deformation pattern prediction from the elastic analysis, corresponding to Point C in Fig. 12a, is shown in Fig. 12d. Computational convergence problems were encountered in the elastic-plastic analysis at Point B, which prevented prediction of the response further into the postbuckling load range. The postbuckled deformation pattern predicted by the elastic-plastic analysis is very similar to the deformation pattern labeled C in the elastic, transient analysis shown in Fig. 11. These results suggest that for the cylinder studied, yielding of the aluminum will prevent the postbuckled deformation pattern predicted by the elastic analysis from developing. This suggestion is consistent with the experimentally observed behavior. The initial postbuckled deformation pattern for the 0.040-inch-thick cylinder with a 3.0-inch-long crack observed in the experiment and shown in Fig. 13a is very similar to the postbuckled deformation pattern predicted by the elastic-plastic analysis, and shown in Fig. 13b.

The predicted prebuckling and buckling analysis results and the measured results for the 0.040-inch-thick shells with crack lengths of 2.0, 3.0, and 4.0 inches are shown in Fig. 14. The analysis predictions were obtained using a material nonlinear analysis. Shell wall imperfections were not measured. An initial geometric imperfection in the form of the lowest eigenmode was used in the nonlinear analysis to generate local deformations in the vicinity of the crack. The measured loading-platen displacements were used to determine the amount of end rotations of the shell, and these data were used as input loading parameters for the nonlinear analysis. Buckling of each of the shells is identified by the symbols in Fig. 14. The filled symbols correspond to the analytical buckling predictions, and the open symbols correspond to the experimentally

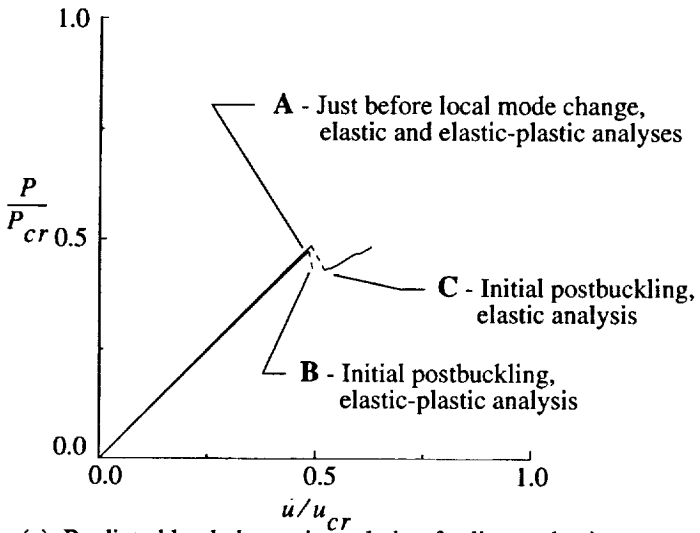

(a) Predicted load-shortening relation for linear-elastic response and material-nonlinear response

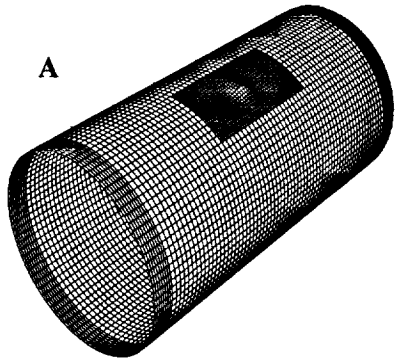

(b) Predicted deformation pattern just before local mode change, for linear-elastic response and material-nonlinear response (Point A)

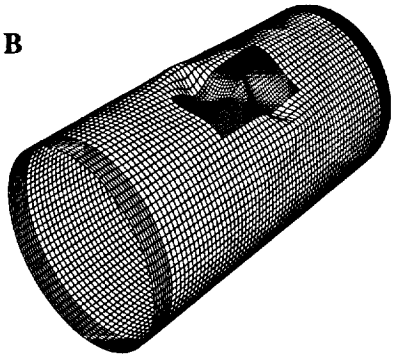

(c) Predicted initial postbuckling deformation pattern for material-nonlinear response (Point B)

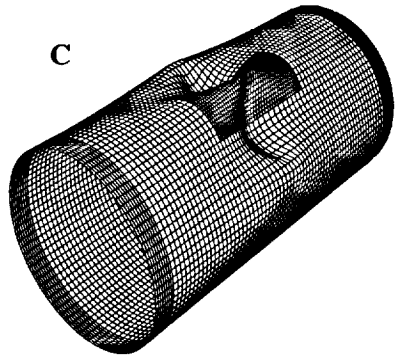

(d) Predicted initial postbuckling deformation pattern for linear-elastic response (Point C)

Figure 12. Comparison of linear-elastic and material-nonlinear responses of a 0.040-inch-thick shell with a 3.0-inch-long crack and subjected to axial compression.

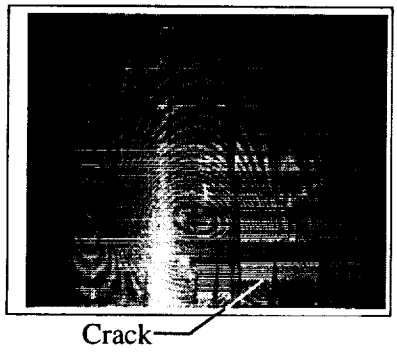

(a) Measured postbuckling deformation

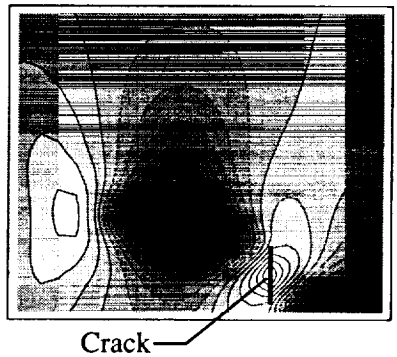

(b) Predicted postbuckling deformation

Figure 13. Comparison between measured and predicted postbuckling response at Point B, on Fig. 12a.

measured buckling loads. For the shell with the 2.0-inch-long crack, the predicted and measured general instability occurred at the loads indicated by the squares in Fig. 14. For the shells with the 3.0- and 4.0-inch-long cracks, the symbols indicate the load at which there was a change in the local buckling mode. The results shown in Fig. 14 indicate that the analytical results slightly overestimate the experimental results for the buckling loads, but slightly underestimate the shell stiffness. The discrepancies in the presented analytical and experimental results could be a result of uncertainties in the loading platen end rotations, shell wall imperfections, and other differences in the analytical model and the as-tested specimens.

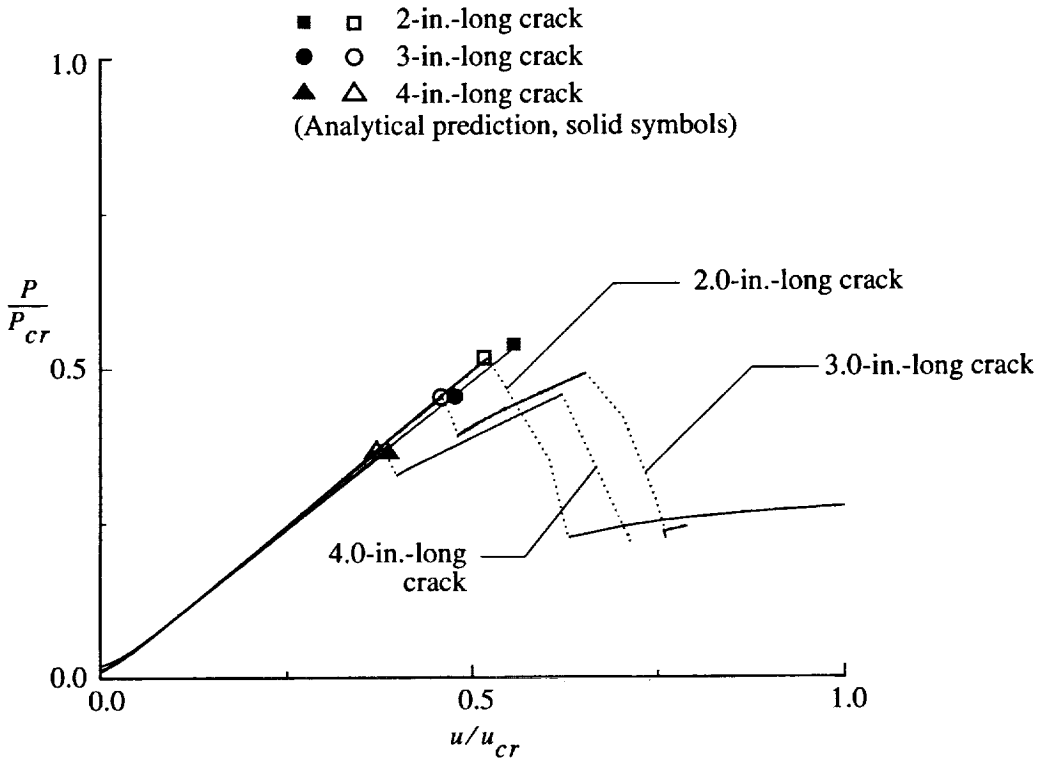

Figure 14. Summary of predicted and experimental load-shortening relations for 0.040-inch-thick shells subjected to axial compression.

CONCLUDING REMARKS

The results of an analytical and experimental study of the effects of a longitudinal crack on the nonlinear response of thin, unstiffened, aluminum cylindrical shells subjected to internal pressure and axial compression loads are presented. The results indicate that the nonlinear response of a shell depends on the loading condition applied to the shell and the initial crack length. The magnitude of the internal pressure required to initiate stable crack growth in a shell subjected to internal pressure decreases as the initial crack length increases. The magnitude of the internal pressure required to cause unstable crack growth in a shell also decreases as the initial crack length increases. The effects of crack length on the prebuckling, buckling and postbuckling responses of typical shells subjected to axial compression loads are also described. The initial buckling load of a shell subjected to axial compression decreases as the initial crack length increases. Initial buckling causes general instability or collapse of a shell for shorter initial crack lengths. Initial buckling is a stable local response mode for longer initial crack lengths. This stable local buckling response is followed by a stable postbuckling response, which is followed by general or overall instability of the shell.

REFERENCES

[1]Starnes, J., H., and Rose, C., A., "Nonlinear Response of Thin Cylindrical Shells with Longitudinal Cracks and Subjected to Internal Pressure and Axial Compression Loads," AIAA Paper No. 97-1144, April 1997.

[2]Newman, J. C., Jr., "An Elastic-Plastic Finite Element Analysis of Crack Initiation, Stable Crack Growth and Instability," ASTM STP 833, 1984, pp. 93-117.

[3]Brogan, F. A., Rankin, C. C., and Cabiness, H. D., "STAGS User Manual, Version 3.0," Lockheed Martin Missiles and Space Co., Inc., Advanced Technology Center, Report LMMS P032594, June, 1998.

[4]Riks, E., "Some Computational Aspects of the Stability Analysis of Nonlinear Structures," Computational Methods in Applied Mechanics and Engineering, Vol. 47, 1984, pp. 219-259.

[5]Riks, E., "Progress in Collapse Analysis," Journal of Pressure Vessel Technology, Vol. 109, 1987, pp. 27-41.

[6]Rankin, C. C., Brogan, F. A., and Riks, E., "Some Computational Tools for the Analysis of Through Cracks in Stiffened Fuselage Shells," Computational Mechanics, Springer International, Vol. 13, No. 3, December 1993, pp. 143-156.

[7]Dawicke, D. S., Sutton, M. A., Newman, J. C., Jr., and Bigelow, C. A., "Measurement and Analysis of Critical CTOA for an Aluminum Alloy Sheet," NASA TM-109024, September, 1993.

[8]Newman, J. C., Jr., Dawicke, D. S., Sutton, M. A. and Bigelow, C. A., "A Fracture Criterion for Widespread Cracking in Thin-Sheet Aluminum Alloys," Proceedings of the ICAF 17th Symposium, 1993.

[9]Dawicke, D. S., Newman, J. C., Sutton, M. A., and Amstutz, B. E., "Stable Tearing Behavior of a Thin-Sheet Material with Multiple Cracks," NASA TM-109131, July, 1994.

[10]Shivakumar, K. N., and Newman, J. C., Jr., "ZIP3D - An Elastic-Plastic Finite-Element Analysis Program for Cracked Bodies," NASA TM-102753, 1990.

[11]Dawicke, D. S., and Newman, J. C., Jr., "Residual Strength Predictions for Multiple Site Damage Cracking Using a Three-Dimensional Finite Element Analysis and a CTOA Criterion," Fatigue and Fracture Mechanics: 29th Volume, ASTM, STP 1332, T. L. Panontin, and S. D. Sheppard, Eds., American Society for Testing and Materials, 1998.

[12]Newman, J. C., Jr., "Finite Element Analyses of Fatigue Crack Propagation -- Including the Effects of Crack Closure," Ph.D. Thesis, Virginia Polytechnic Institute and State University, Blacksburg, VA, May 1974.

[13]Dawicke, D. S., "Residual Strength Predictions Using a Crack Tip Opening Angle Criterion," FAA-NASA Symposium on the Continued Airworthiness of Aircraft Structures, DOT/FAA/AR-97/2, Vol. II, July 1997, pp. 555-566.

[14]Riks, E., Brogan, F. A., and Rankin, C. C., "Bulging of Cracks in Pressurized Fuselages: A Procedure for Computation," in Analytical and Computational Models of Shells, Noor, A. K., Belytschko, T., and Simo, J. C., Eds., The American Society of Mechanical Engineers, ASME-CED Vol. 3, 1989.